NASA/TM—2020-220519

On-Orbit Validation of a Framework for Spacecraft-Initiated Communication Service Requests With NASA's SCaN Testbed

Adam M. Gannon, Dale J. Mortensen, Marie T. Piasecki, and Joseph A. Downey
Glenn Research Center, Cleveland, Ohio

March 2020

NASA STI Program . . . in Profile

Since its founding, NASA has been dedicated to the advancement of aeronautics and space science. The NASA Scientific and Technical Information (STI) Program plays a key part in helping NASA maintain this important role.

The NASA STI Program operates under the auspices of the Agency Chief Information Officer. It collects, organizes, provides for archiving, and disseminates NASA's STI. The NASA STI Program provides access to the NASA Technical Report Server—Registered (NTRS Reg) and NASA Technical Report Server—Public (NTRS) thus providing one of the largest collections of aeronautical and space science STI in the world. Results are published in both non-NASA channels and by NASA in the NASA STI Report Series, which includes the following report types:

- TECHNICAL PUBLICATION. Reports of completed research or a major significant phase of research that present the results of NASA programs and include extensive data or theoretical analysis. Includes compilations of significant scientific and technical data and information deemed to be of continuing reference value. NASA counter-part of peer-reviewed formal professional papers, but has less stringent limitations on manuscript length and extent of graphic presentations.

- TECHNICAL MEMORANDUM. Scientific and technical findings that are preliminary or of specialized interest, e.g., "quick-release" reports, working papers, and bibliographies that contain minimal annotation. Does not contain extensive analysis.

- CONTRACTOR REPORT. Scientific and technical findings by NASA-sponsored contractors and grantees.

- CONFERENCE PUBLICATION. Collected papers from scientific and technical conferences, symposia, seminars, or other meetings sponsored or co-sponsored by NASA.

- SPECIAL PUBLICATION. Scientific, technical, or historical information from NASA programs, projects, and missions, often concerned with subjects having substantial public interest.

- TECHNICAL TRANSLATION. English-language translations of foreign scientific and technical material pertinent to NASA's mission.

For more information about the NASA STI program, see the following:

- Access the NASA STI program home page at http://www.sti.nasa.gov

- E-mail your question to help@sti.nasa.gov

- Fax your question to the NASA STI Information Desk at 757-864-6500

- Telephone the NASA STI Information Desk at 757-864-9658

- Write to:
  NASA STI Program
  Mail Stop 148
  NASA Langley Research Center
  Hampton, VA 23681-2199

NASA/TM—2020-220519

On-Orbit Validation of a Framework for Spacecraft-Initiated Communication Service Requests With NASA's SCaN Testbed

Adam M. Gannon, Dale J. Mortensen, Marie T. Piasecki, and Joseph A. Downey
Glenn Research Center, Cleveland, Ohio

National Aeronautics and
Space Administration

Glenn Research Center
Cleveland, Ohio 44135

March 2020

Acknowledgments

The authors acknowledge Gus Gemelas, Jason Murray, Steve Paulus, Dean Schrage, and Larry Vincent for develop-ment of the UIS automation software discussed in this work. Leveraging existing code developed by Mike Evans, Mary Jo Shalkhauser, Nick Tollis, and Bryan Welch was critical to meeting a compressed development schedule. Ray Lotenero and Al Tucholski aided in fabrication of RF equipment. We acknowledge the contributions of Jacob Barnes, Jacob Burke, Dave Chelmins, David Israel, Robert Morgenstern, Rich Reinhart, Chris Roberts, and Mark Sinkiat in defining and refining the UIS concept. Finally, the SCaN Testbed operations team particularly Helen Brown and Beth Curtis were critical to the success of this experiment.

Level of Review: This material has been technically reviewed by technical management.

Available from

NASA STI Program
Mail Stop 148
NASA Langley Research Center
Hampton, VA 23681-2199

National Technical Information Service
5285 Port Royal Road
Springfield, VA 22161
703-605-6000

This report is available in electronic form at http://www.sti.nasa.gov/ and http://ntrs.nasa.gov/

On-Orbit Validation of a Framework for Spacecraft-Initiated Communication Service Requests With NASA's SCaN Testbed

Adam M. Gannon, Dale J. Mortensen, Marie T. Piasecki, and Joseph A. Downey
National Aeronautics and Space Administration
Glenn Research Center
Cleveland, Ohio 44135

***Abstract*—We design, analyze, and experimentally validate a framework for demand-based allocation of high-performance space communication service in which the user spacecraft itself initiates a request for service. Leveraging machine-to-machine communications, the automated process has potential to improve the responsiveness and efficiency of space network operations. We propose an augmented ground station architecture in which a hemispherical-pattern antenna allows for reception of service requests sent from any user spacecraft within view. A suite of ground-based automation software acts upon these direct-to-Earth requests and allocates access to high-performance service through a ground station or relay satellite in response to immediate user demand. A software-defined radio transceiver, optimized for reception of weak signals from the helical antenna, is presented. Design and testing of signal processing equipment and a software framework to handle service requests is discussed. Preliminary results from on-orbit demonstrations with a testbed onboard the International Space Station are presented to verify feasibility of the concept.**

I. Motivation

EFFICIENCY and reconfigurability are necessary attributes of space communication networks tasked to support scientific and exploration missions with increasingly complex objectives and dynamic communications needs. As a growing number of spacecraft are outfitted with more numerous and increasingly complex instruments, improved communications network autonomy is required to meet increased bandwidth and capacity requirements. Ideally, the space communications infrastructure is able to autonomously balance resources to exactly meet each user's immediate demand.

An increasingly varied communications infrastructure consisting of government, commercial, and academic services presents a wide variety of data transfer options to a user spacecraft. The heterogeneity of potential wireless links makes broad generalizations difficult. However, it is fundamental to communications engineering that the characteristics of each link represent a trade-off between availability and performance [1]. *High-availability* links are designed to maximize coverage or number of simultaneous users. This goal often necessitates a multiple access scheme which divides resources (i.e. in the time, frequency, or code domains) and limits per-user capacity. *High-performance* links which offer the highest data rates (or, equivalently, minimize design requirements of the user spacecraft) generally feature large apertures and high-performance electronics. Associated costs place a limit on the number of deployments and necessitates sharing of assets across many users with a scheduling process to balance demand.

In current practice, the process of scheduling communications service begins with a human mission operator initiating a request. For assets in high demand this process may begin weeks in advance. The mission operator must anticipate future data transfer needs which may change significantly in the interim. An increasing number of spacecraft have time-varying and low-latency service requirements to execute trajectory corrections or adjust mission operations in response to changing circumstances. For example, spacecraft engaged in transient science, observations of natural phenomena whose occurrence is difficult or impossible to anticipate, collect large volumes of unanticipated science data which must be offloaded before onboard data storage is exhausted [2], [3], [4]. Consider a recent binary neutron star merger first observed through the terrestrial LIGO and Virgo detectors [5]. An extensive observation campaign began in the hours to days after detection involving no fewer than a dozen orbiting instruments, many of which communicate through the Space Communications and Navigation (SCaN) networks operated by the National Aeronautics and Space Administration (NASA).

With multiple users competing for limited assets, high-performance links are generally managed by human schedulers who manually resolve conflicts among scheduling requests submitted by human mission operators. This limits the network's ability to rapidly renegotiate schedules. In this paradigm, the cost to mission and network operations increases as more missions come online. This goes contrary to the trend in science missions that envisions small satellites, which are cheaper to build and operate, increasingly performing Decadal-class science [6]. Future space communications architecture envisions high-bandwidth relays in orbit around other bodies such as the Moon and Mars to support complex multi-vehicle science and exploration objectives [7], [8]. The increased commanding latency and reduced bandwidth that arises from moving high-performance links further into the solar system exacerbates the scheduling issue requiring more autonomy for efficient operations.

The concept of user-initiated service (UIS) originated from the desire to provide more responsive access to high-performance space communications links [7], [10], [11]. In this

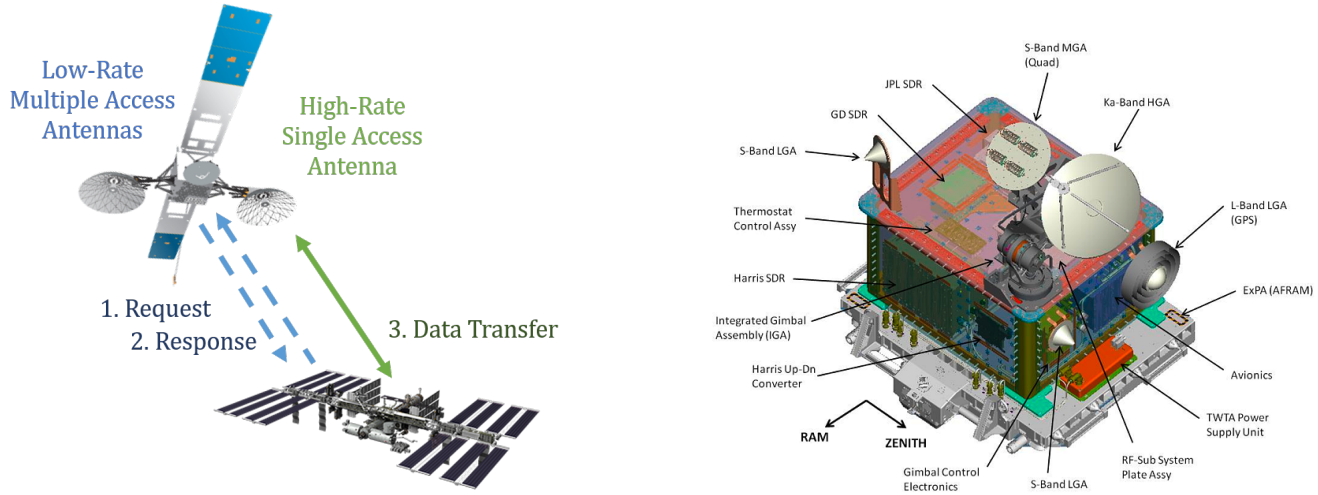

(a) (b)

Fig. 1: (a) UIS operations demonstrated in [9]. Requests for service were relayed through low-rate multiple access antennas on a TDRS. Once access was granted, high-rate data transfer occurred through a single access antenna. (b) SCaN Testbed.

new paradigm, the end user (the spacecraft itself) originates the request based on current communication service needs. The scheduling process is highly automated employing machine-to-machine communications for requests and responses from the network. This architecture of automated resource allocation can be thought of as a "Space Mobile Network", producing a user experience analogous to that of a terrestrial mobile network [1], [10]. Of course, legacy support for requests initiated by mission operators is continued and manual operations capability remains an option to ensure mission success during critical events and spacecraft emergencies. However, for normal operations the UIS concept increases responsiveness of shared resources to meet changing demand and improves network efficiency through increased autonomy.

II. Background

From the physical layer view, the UIS concept can be summarized as a framework over which access to high-performance links can be requested by sending UIS requests over low-rate, high-availability links. Employing a common control channel to request radio resources from a network is seen in the base station association process in terrestrial wireless or the hailing channel specified in the Proximity-1 protocol used by spacecraft in the vicinity of Mars [1], [12], [13]. To be useful, the control channel must be accessible by all users and able to handle requests that may come at any time. Such a control channel exists in the multiple access service provided by NASA's Tracking and Data Relay Satellite (TDRS) System and was the basis of an initial flight demonstration of the user-initiated service capability [9].

A conceptual diagram of the demonstration is shown in Fig. 1a. The S-band multiple access service provided by a TDRS was used to relay low-rate UIS requests from SCaN Testbed on the International Space Station (ISS). Once the request was handled through an automated process, a Ka-band single access relay link was allocated to SCaN Testbed for data return. Though both relay services were provided by a TDRS, the high-performance Ka-band link supports data rates over 3 orders of magnitude greater than the S-band multiple access service. The following sections describe elements of this architecture in detail.

A. SCaN Testbed

SCaN Testbed (Fig. 1b) was a software-defined radio (SDR) platform used to advance adaptive and intelligent space communications technologies through on-orbit demonstrations. Flown as an external experiment on ISS from 2012 – 2019, SCaN Testbed hosted three SDRs each capable of being reprogrammed to run different waveforms [14]. Thus, each device could test hundreds of experimental physical- and upper-layer protocols simply by uploading new software while on orbit. The design evaluated in this work was tested on the S-band SDR built in partnership with NASA Jet Propulsion Laboratory (JPL) and L3 Cincinnati Electronics (referred to hereafter as the JPL SDR).

The experiment hosted three antennas for communications over the NASA Space Network: two steered (medium gain at S-band and high gain at Ka-band) and one S-band low-gain hemispherical antenna fixed in a zenith-facing direction. An additional S-band low-gain hemispherical antenna was mounted in the nadir-facing direction for direct-to-Earth communications over the NASA Near Earth Network and the S-Band Ground Station at NASA Glenn Research Center (GRC) in Cleveland, Ohio, USA.

B. NASA's Space Network

The NASA Space Network comprises a constellation of TDRS relays in geosynchronous orbit (at an altitude of approximately 35,800 km) and their associated ground stations. The satellites operate as "bent-pipe" relays, transferring signals between spacecraft in Earth orbit and ground stations

Byte	Description	Byte	Description
0	Protocol Version	13	Service Urgency (1-10)
1-2	Destination Identifier	14-17	Data Size (bytes)
3-4	Source Identifier	18-21	Suggested Minimum Event Duration (minutes)
5	Service Type & Transaction Type	22-25	Suggested Maximum Event Duration (minutes)
6	Message Type	26-29	Required Minimum Event Duration (minutes)
7	Flags	30-49	Suggested Asset (e.g. TDRS-10, WS1)
8	Service Identifier	50-53	Suggested Radio Settings Identifier
9	Message Sequence Number	54-57	Required Communications Start (Unix timestamp of latest allowable time)
10-11	Message Length (bytes)	58-61	Current Schedule Data Checksum
12	Header Checksum	62	Multiple Event Flag
		63	Immediate Request Flag
		64	Message Checksum

TABLE I: UIS Request Format. The left column describes the header common to all UIS messages. The right column is specific to the request and provides information which aids the scheduling process.

connected to terrestrial Internet. Each TDRS is equipped with two mechanically-steered parabolic dish antennas which operate at S-band, Ku-band, and Ka-band. These antennas allow data rates up to 1.5 Gbps at Ka-band but their narrow beamwidth generally limits each antenna to supporting only one spacecraft at a time [15]. Each TDRS is able to support an additional number of simultaneous users through a grid of fixed S-band antenna elements. A beamforming network uses a spacecraft's orbital state vector to track a spacecraft via electronic steering of antenna elements while spreading codes unique to each spacecraft provide a multiple access scheme. This allows for forward and return service to multiple spacecraft simultaneously[1].

The Demand Access System (DAS) allows for expansion of multiple access return services including the capability to schedule service for an extended duration. The DAS provides multiple access return service to two classes of users: dedicated and non-dedicated [16]. Dedicated user spacecraft are provided continuous 24/7 coverage while mission operators of non-dedicated user spacecraft can manually request on-demand service through a software interface with as little as 30 seconds notice [15]. In order to support 24/7 access, beamformers are assigned constantly to dedicated DAS users, regardless of how infrequently they actually demodulate data. Availability of beamformers places a limit on the number of simultaneous users per TDRS [17]. However, since beamforming is done on the ground, additional hardware can expand the system to support more users. While able to cover a wide area and support a number of simultaneous users, the service can only provide a maximum of 300 kbps to any one spacecraft [15].

Apart from the DAS, scheduling of other Space Network services occurs through the Network Control Center Data System (NCCDS). The NCCDS forecast scheduling process begins at least 14 days in advance with priority-based allocation of requests submitted by mission operations staff to the NCCDS [15]. After the forecast scheduling process has concluded requests can still be accepted, up to 10 minutes in advance of an access, and automatically scheduled in gaps around currently reserved accesses on a first-come first-served basis [15]. To aid this process, periods of time when a given TDRS is not in use are regularly published to a server. The initial flight demonstration of UIS built upon these existing dynamic scheduling capabilities. SCaN Testbed's request for high-rate service was sent through the DAS. Upon receiving the request, ground software interacted with the Space Network scheduling system to reserve unused time. This process is detailed in Section II-D.

C. NASA's Ground Stations

The NASA Near Earth Network (NEN) provides coverage for spacecraft in Earth and lunar orbit through a network of ground stations on all seven continents. These assets provide high-performance links through dish antennas up to 18 m in diameter [18]. Each dish uses mechanical steering to track a spacecraft during a line-of-sight pass. At the orbit of ISS a pass typically lasts approximately 5 minutes. Due to narrow beamwidth, these ground stations are typically single access assets[2].

To support SCaN Testbed operations, particularly the experimental waveforms tested on-board, NASA commissioned a 2.4 m S-band ground station at Glenn Research Center (hereafter the GRC GS) [19]. Per spectrum authorization the ground station is a co-primary user of the 2025 – 2110 MHz band, requiring coordination with Cleveland-area radio and television broadcasters to protect their services [20]. Radiated power is limited to a maximum 10 W at antenna boresight. Furthermore, the antenna cannot radiate at elevation angles less than 10°. The GRC GS has operated regularly since 2015 without any known instances of interference towards area broadcasters.

D. UIS Requests Through the Space Network

The work presented here builds upon a 2017 experiment using SCaN Testbed [9]. In summary, steps of this experiment were:

1) Several weeks before the experiment, a multiple access forward TDRS link is requested for the duration of the experiment through the NCCDS.

[1] A forward link denotes the link from a service provider to a user spacecraft, consisting of both an uplink to the relay satellite and downlink to the user. A return link is the opposite: carrying data from a user spacecraft to the network.

[2] Spacecraft flying in close formation in low-Earth orbit (such as CubeSat clusters) or spacecraft at a much greater distance from Earth (such as in lunar orbit) could potentially simultaneously fit within the 3 dB beamwidth of a ground station antenna.

2) Minutes before the experiment, SCaN Testbed (a non-dedicated DAS user) is allocated a DAS beamformer for the duration of the experiment. A network interface is opened to forward received packets from the DAS to the Event Manager, a ground-based software application described in Section III.
3) SCaN Testbed, emulating a science mission in need of high-rate communication services to downlink data, formats a UIS request packet (see Table I).
4) SCaN Testbed sends the UIS request packet to a TDRS where it is relayed to the ground and forwarded to the Event Manager over terrestrial Internet.
5) The Event Manager begins to process the request. Tempus, a software application developed to interface with the Space Network scheduling system, is used to request unused time on a TDRS single access dish at Ka-band.
6) With the access granted, the Event Manager forms an instruction set from which SCaN Testbed can determine access and pointing to the TDRS high-gain antenna.
7) The UIS response containing the instruction set is sent over the legacy multiple access forward service and is received by SCaN Testbed.
8) SCaN Testbed uses the received instruction set to determine the event start time, stop time, and antenna pointing instructions. At the start of the access, SCaN Testbed transmits data to the TDRS single access dish at Ka-band.
9) TDRS relays the data to the ground where it is forwarded back to the SCaN Testbed mission operations center through terrestrial Internet.

While representing a significant advancement in the readiness of the technology and the first demonstration of spacecraft-initiated service in Earth orbit, several steps required human intervention in order to make use of existing technology. First, as an experimental platform, SCaN Testbed was registered as a non-dedicated DAS user and required advance scheduling to allocate a DAS beamformer for the duration of the experiment. Without active DAS service the UIS request SCaN Testbed transmitted to a TDRS would not have been received. In an operational UIS system, it is envisioned all user spacecraft using a TDRS as a control channel will be dedicated DAS users with continuously-allocated beamforming hardware. Supporting the hundreds of future spacecraft which will operate in Earth orbit will require additional investment to expand the capacity of the dedicated DAS beamforming system [17].

The UIS concept envisions that an on-demand broadcast service will provide the forward link from TDRS to the user spacecraft over which the UIS responses can be sent [7], [9]. Such a broadcast service will be able to send low-rate data packets to many simultaneous users in Earth orbit [21]. In the absence of an operational forward broadcast service, it was necessary to manually schedule TDRS multiple access forward service to provide a path for the UIS response.

These existing limitations raise the question of alternative low-rate links to transport UIS requests and responses. It is logical to explore the possibility of using the wide coverage of NASA's ground station network to receive these requests.

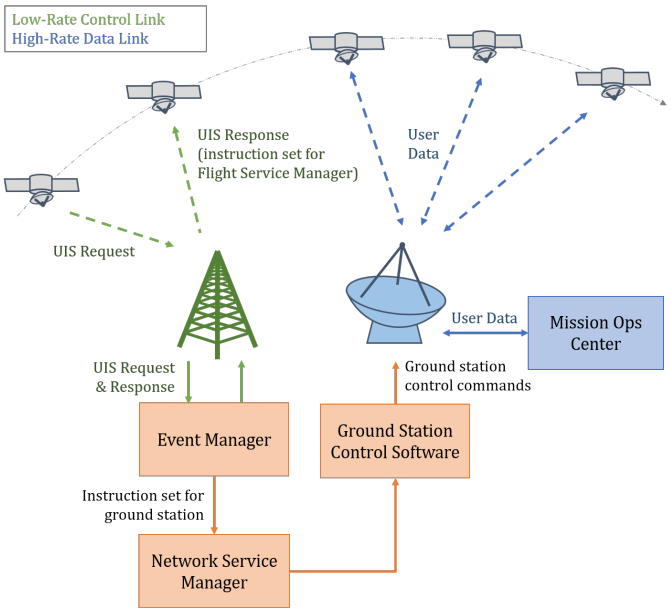

Fig. 2: Overview of direct-to-Earth UIS request process.

Furthermore, available ground stations could be scheduled for high-rate data transfer during the same pass. This expands the flexibility of UIS, including supporting less-capable small satellites without sufficient transmit power to close a link to TDRS (this scenario is analyzed in Appendix A).

This work will explore the direct-to-Earth UIS concept and present results from preliminary flight experiments with SCaN Testbed. Section III describes the system architecture including how ground software components handle service requests and responses. Section IV describes the RF design of the control channel and Section V presents experimental results measuring its RF performance. Finally, Section VI describes the development of a low-rate waveform for the control channel with preliminary results from its characterization presented in Section VII.

III. System Architecture

A summary diagram of the direct-to-Earth UIS request process is shown in Fig. 2. The UIS software suite which enables automation consists of several server-side components on the ground and a client-side component on each user spacecraft.

A. Request Process

The request process begins with a user spacecraft in need of service from the network. Most often this will involve the need for data downlink, though all SCaN services including radiometric tracking for navigation can be supported [9]. The Flight Service Manager (FSM), a software component on the user spacecraft which can be thought of as the client-side application, is used to generate the request. Upon receiving a command from the spacecraft's command and data handling subsystem, the FSM uses an onboard orbit propagator to generate times when line-of-sight access to a ground station exists. The FSM could also provide antenna pointing

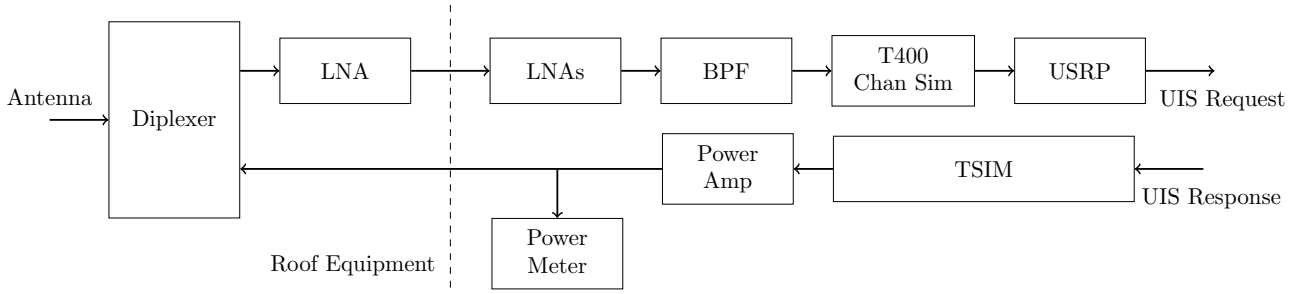

Fig. 3: Summary of RF equipment connected to the hemi antenna for both TX and RX of the control channel. A few components are located on the roof in a waterproof enclosure with the rest of the equipment inside the building.

and Doppler pre-compensation information to the spacecraft's RF subsystem, as discussed in Section VI-A. Finally, the FSM generates a UIS request packet following the structure described in Table I and passes it to the spacecraft's RF subsystem for transmission[3].

At the physical layer, the UIS request packet is sent over a low-rate control channel as described in the following section. Signal processing equipment at the ground station recovers the packet and forwards it over terrestrial Internet to centralized scheduling interface software called the Event Manager (EvM). EvM is capable of interfacing with the scheduling software of other networks such as the Space Network (as in Section II-D) or, in the future, commercial ground stations. It is also itself capable of allocating spacecraft to assets which don't have an existing automated scheduling interface (e.g. a network of ground stations). Thus, direct-to-Earth UIS requests can be used to schedule any space communication asset including relay satellites. In this scenario we focus on scheduling of a high-performance ground station dish. EvM, containing its own orbit propagator, solves for the periods of time when both the user spacecraft is in view and the ground station is available. Schedules are made to optimize priority, urgency, and data volume. EvM can allocate a ground station further downrange in the spacecraft's orbit, on a future orbit, or (based on availability) allow the spacecraft to immediately downlink data to the ground station it sent the UIS request to while still overhead. After allocating an access window to the requesting user spacecraft, the Event Manager must relay this information to both the user spacecraft and the ground station itself.

Rather than replying with explicit timing and antenna pointing information, the UIS response contains an instruction set informing the Flight Service Manager how to generate this information on the spacecraft itself. An advantage of this approach is that the instruction sets can be as small as a few hundred bytes. The very small data volume means a response can be uploaded in a fraction of a second even at very low data rates. After receiving the instruction set, the FSM informs the spacecraft's RF subsystem when it can begin transmitting data. On the ground, the Event Manager communicates with a Network Service Manager which routes the instruction set to the selected ground station through terrestrial Internet. At the designated start time, the high-gain ground station dish slews to track the user spacecraft and forwards received data to the mission operations center.

[3]Before a spacecraft can send requests to a ground station for the first time it must first send a subscription request message. See [9] for more details.

B. Control Plane Physical Link

In the concept of operations discussed above, any spacecraft within line-of-sight range of a ground station can send a UIS request. This presents a challenge to using highly directional parabolic antennas to receive these requests. Before a request is sent, the ground station has no knowledge of which (if any) spacecraft within view will request service. Tracking one spacecraft throughout its pass will prevent the ground station from receiving UIS requests from all other spacecraft. A straightforward solution is the installation of a second antenna at the ground station, particularly one capable of receiving simultaneous requests arriving from any spacecraft within view.

One possible implementation involves using an electronically-steered antenna array to track each potential requesting spacecraft throughout its pass with a low-rate beam [1]. A far simpler solution is to use a fixed position hemispherical-pattern (hemi) antenna to provide coverage over all possible azimuth and elevation angles. This is the approach explored in this work. However, the gain of a wide field of view hemi antenna is 30 dB less than the 2.4 m GRC GS. We can make up the deficit by taking advantage of the small data volumes required by UIS requests and responses. Operating the link at a low data rate of approximately 1 kbps is sufficient to transfer the messages in reasonable time while still closing a link to the hemi antenna. Still, this approach does not leave much link margin to spare requiring a well-designed RF chain connected to the hemi antenna.

IV. RF Design

The hemispherical antenna is colocated with the GRC GS on the roof of a building at NASA Glenn Research Center in Cleveland, Ohio, USA. The majority of signal processing equipment is housed inside the building with a small number of components located on the roof next to the antenna in a waterproof enclosure. Connections between the interior and hemi antenna are through cable runs of LMR-400 producing 7.8 dB of loss. Transmit and receive signals travel through separate cables connected to the common hemi antenna through a diplexer. Figs. 3 and 4 show the RF chain this section will describe in detail.

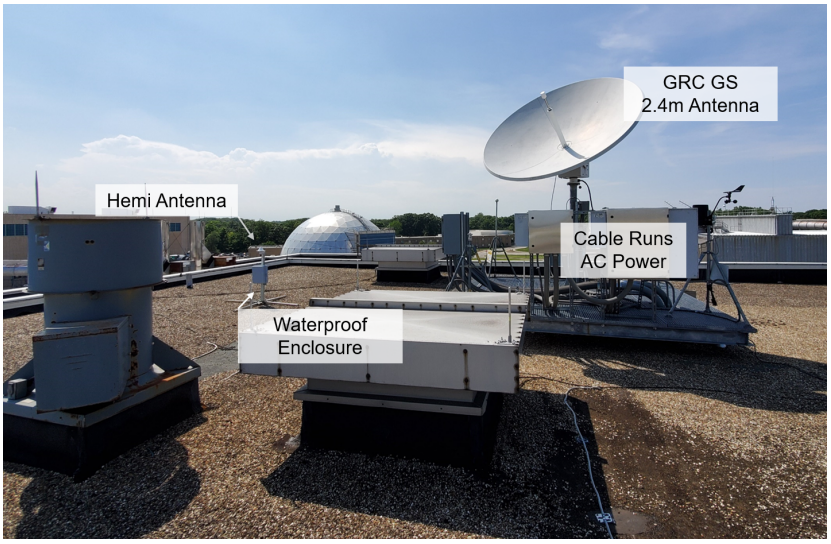

(a)

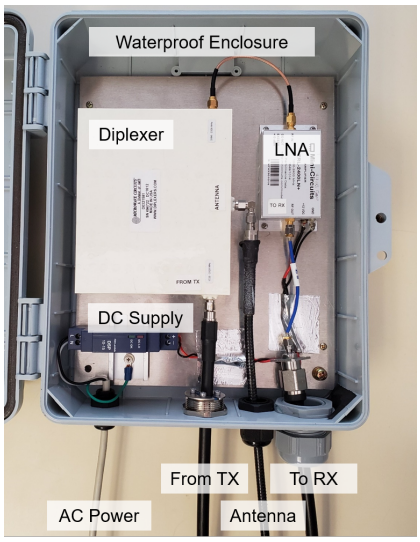

(b)

Fig. 4: (a) Deployment of hemispherical antenna colocated with the 2.4 m dish of the GRC GS on a roof at NASA Glenn Research Center. (b) Detailed view of waterproof enclosure which houses the diplexer and low-noise amplifier.

A. Antenna Selection

The chosen antenna was purchased as a backup to the zenith-facing and nadir-facing low gain antennas during SCaN Testbed integration and testing. The spare antenna, an AS-48915 S-band conical spiral, offers a hemispherical antenna pattern well suited to the wide coverage area required for the control channel. At S-band the antenna provides a 3 dB beamwidth of 90° with maximum gain of 4 dBi [22]. The antenna is mounted on the roof with boresight directed at zenith.

B. Maximum Transmit Power

The limiting factor in transmit power is interference to other S-band users. As a co-primary user, NASA must ensure new transmissions operate without causing interference to existing links, namely those used by terrestrial radio and television broadcasters in the Cleveland area. Therefore the transmit power of the hemi antenna is set such that signal strength towards the horizon is no greater than that currently produced by the GRC GS.

The antenna pattern of the GRC GS shows a maximum gain at antenna boresight of 31.5 dBi. The GRC GS is authorized to steer to elevation angles as low as 10° above the horizon. When the antenna is oriented at 10° elevation, the antenna gain towards the horizon (i.e. 10° off-boresight) is −5 dBi. At the maximum licensed transmit power of 10 W this corresponds to an equivalent isotropically radiated power (EIRP) of 5 dBW. In summary, during the course of normal operations since 2015, the GRC GS has radiated 5 dBW towards the horizon without any noted interruption to receivers of area broadcasters. The EIRP of the hemispherical antenna will be calculated to be no greater than this existing level of tolerable signal strength. Measurements of the hemi antenna show a maximum gain towards the horizon (90° off-boresight) of 0 dBi. Therefore, 5 dBW (3.2 W) of input power to the antenna results in a maximum EIRP at the horizon of 5 dBW.

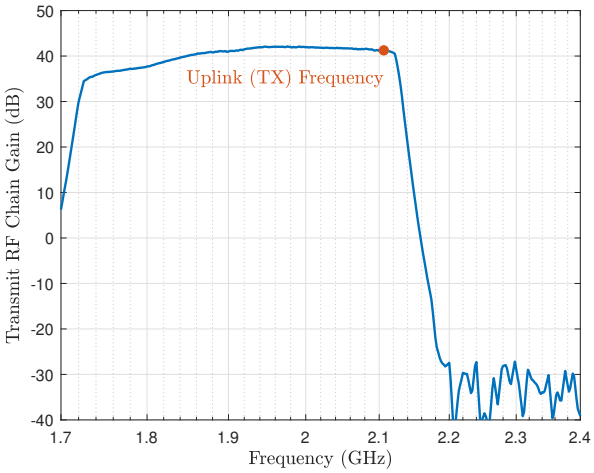

Fig. 5: Measured gain of the transmit chain, from TSIM to antenna, versus frequency.

C. Transmit Hardware

The transmitter used in the experiment is an RT Logic TDRS Simulator (TSIM) which has adjustable transmit power up to +2 dBm. Transmit gain of the TSIM is adjusted to produce exactly 5 dBW at the hemi antenna (verified with a power meter). Fig. 5 shows the measured gain of the TX chain is 41.5 dB at the TX frequency.

A preliminary link budget calculation can be made using the assumptions in Table II and the detailed description of the TX chain in Table III. ISS flight rules restrict the station's apogee to between 280 km and 460 km with 400 km the average. The required energy per bit to noise power spectral density ratio (E_b/N_0) to maintain a bit error rate (BER) of 10^{-5}

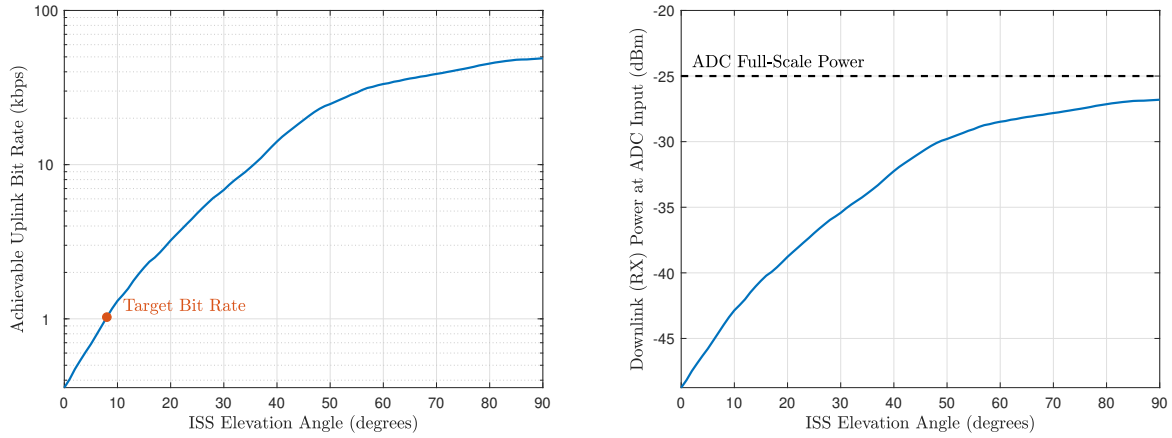

Fig. 6: (a) Achievable uplink (TX) bit rate versus elevation angle while maintaining 2 dB link margin and an average BER of 10^{-5}. The target bit rate is achieved above 8° elevation. (b) Predicted downlink (RX) power at the input of the channel simulator's ADC versus elevation angle. The dashed line indicates the ADC full scale power of −25 dBm.

with $^1/_2$-rate convolutionally-coded binary phase-shift keying (BPSK) is approximately 6.5 dB. While these assumptions remain constant, the TX antenna gain and free-space path loss are a function of elevation angle and will change throughout the pass. Fig. 6a plots the achievable uplink bit rate as a function of elevation angle assuming a desired link margin of 2 dB. The achievable bit rate increases rapidly with elevation angle, reaching a maximum of 50 kbps for the rare case of ISS directly over the ground station. We observe that the target bit rate of 1 kbps can be achieved at any elevation angle above approximately 8°. This verifies that transmitting a UIS response during the beginning of a pass is reasonable. Section V-A calculates more detailed link budgets on a pass-by-pass basis using simulated altitude and orientation of SCaN Testbed.

D. Receive Hardware

We now turn our focus to the downlink. The full RX chain is described in Table IV, which shows a total noise figure of 3.3 dB. Low noise figure was achieved by placing a low-noise amplifier (LNA) as early in the RF chain as possible: particularly before the 7.8 dB attenuation from the 125′ (38 m) cable run. The LNA is housed with the diplexer in a waterproof enclosure on the roof.

The first digital device encountered is the RT Logic T400 Channel Simulator, which is used to compensate for Doppler shift. The analog-to-digital converter (ADC) in the Channel Simulator has a full-scale power of −25 dBm. Quantization noise can be reduced by driving the T400 as close to this level as possible without exceeding it and saturating the ADC. Three amplifiers, two external and one integrated into the T400, are used to boost the weak received signals to an acceptable input power. Using the assumptions in Table II the RF power level at the ADC is plotted as a function of elevation angle in Fig. 6b. We observe the gain is optimized to provide the strongest signal without crossing into saturation.

One final consideration is the RF power transferred from the TX chain to the RX chain through the diplexer. The measured isolation between TX and RX ports on the diplexer is 90.8 dB. However, this still produces a signal level of +4.9 dBm at the output of the second ZRL-2300, slightly higher than the 0 dBm maximum input power to the T400. A band-pass filter is used to provide an additional 14.7 dB attenuation at the TX frequency while only slightly attenuating the RX signal. This brings the TX signal to a safe −9.8 dBm of input power to the T400, where the downconversion and filtering stages remove it from the intermediate frequency input to the ADC.

A link budget analysis with the assumptions in Table II shows that the target bit rate of 1 kbps is achievable at any elevation above 6°. Combined with the results in Fig. 6a it seems feasible that a spacecraft can both send a UIS request and receive a UIS response during the beginning of its pass over a ground station.

Parameter	Value
TX Power into Hemi Antenna	5 dBW
SCaN Testbed EIRP	7.5 dBW
SCaN Testbed G/T	−28.4 dB/K
ISS Altitude	400 km
Atmospheric & Rain Attenuation	0.5 dB
Required E_s/N_0	6.5 dB

TABLE II: Link budget assumptions.

V. RF Performance

It was realized that testing both new RF hardware and a new SDR waveform on one flight experiment would make it difficult to isolate the cause of any problems. This necessitated an initial flight experiment to evaluate the performance of the hemi antenna and RF equipment. An initial flight experiment could be pursued in parallel to waveform development and

Order	Component	Function	Gain (dB)	Power Level (dBm)
1	RT Logic TDRS Simulator	Transmit radio	-	-6.3
2	Mini-Circuits ZHL-100W-242+	Power amplifier	51	44.7
3	Narda 4013C-20	Directional coupler for power meter	-0.2	44.5
4	100′ LMR-400	Coaxial cable from indoors to roof	-6.0	38.5
5	25′ LMR-400	Coaxial cable along roof to diplexer	-1.8	36.7
6	Microwave Circuits D0321581	Diplexer	-1.0	35.7
7	8′ FSJ1-50A	Coaxial cable from diplexer to antenna	-0.7	35.0
		Total	**41.3**	**35.0**

TABLE III: Transmit chain components.

reduce risk for the final flight experiment. During this experiment, SCaN Testbed sent and received signals to and from the hemi antenna using an existing waveform. This section presents measurements from this initial flight experiment and compares them to link budget predictions.

A. Detailed Predictions

While simple link budget analyses such as the one in Fig. 6a are sufficient for the purposes of planning and RF chain design, higher fidelity models are required to perform analysis on a pass-by-pass basis. Pre-flight testing characterized the response of the nadir-facing low-gain antenna in isolation. However, its antenna response is quite different when integrated with the complex ground plane of SCaN Testbed. Recognizing that the success of future experiments would depend on a reliable characterization of the RF environment, the SCaN Testbed team performed an extensive in-situ characterization of the antenna response when on-orbit [23]. These measurements were integrated into the SCaN Testbed Analysis Tool (STAT), a prediction utility developed to aid experiments.

STAT ingests two-line element sets regularly updated by ISS operations. Propagating the space station's orbit, the tool predicts times when the ISS will be in view of the GRC GS. Since the space station is a complex structure with potential obstructions during the pass, STAT includes a three-dimensional model of the station from which reduced signal level due to blockages can be estimated. By combining orbital mechanics simulation with antenna measurements STAT can create pass-by-pass predictions of bidirectional RF signal strength. From these predictions, key link performance parameters such as E_b/N_0 and BER can be estimated. By default STAT assumes a link between SCaN Testbed and the GRC GS, making it necessary to modify the tool to include the hemi antenna and signal processing equipment.

B. Waveform Selection

The initial flight experiment took place in parallel to SDR waveform development, requiring the use of an existing waveform. During initial checkout of SCaN Testbed, a TDRS-compatible waveform developed in collaboration with NASA Goddard Space Flight center was used to characterize the JPL SDR. The Glenn-Goddard-TDRS (GGT) waveform [24], [25] offers a low rate mode which transmits 18 kbps in the uplink direction and 24 kbps in the downlink. Obviously 24 kbps is significantly higher than the design rate of 1 kbps and requires an additional 13.8 dB margin to close a link under the same conditions. This makes the waveform unusable for UIS requests and responses during most passes. However, occasionally ISS will pass at a high elevation angle producing greatly increased signal strength. Data in this section is from one such particularly strong pass with sufficient margin to close the link at the higher data rate of the GGT waveform.

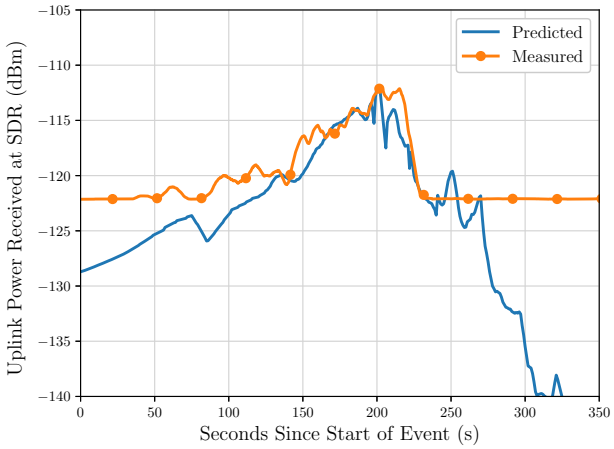

Fig. 7: Measured received signal power in the uplink, averaged over a 10 s window, versus predicted power from STAT. Note the measurement has a lower limit of −122 dBm.

C. Results

The modified STAT provided a prediction of the pass. The RF chain can be verified in two ways: by comparing the predicted RF power to measured RF power and by comparing measured BER to the expected bit error rate as a function of predicted E_b/N_0.

The GGT waveform records an estimate of the received signal power at the input of the SDR which is valid down to −122 dBm. Fig. 7 shows the uplink power received by the JPL SDR during the pass. Power gradually increases from 100 s − 200 s as the approaching ISS reduces the path loss. Power rapidly drops off during the second half of the pass as the signal received is now from the back lobe of the transmitting antenna. The measurement is valid in the approximate range of 40 s − 230 s during which the signal is above the measurement floor. Throughout this range we observe strong agreement between the predicted and measured power.

Order	Component	Part Number	Noise Figure (dB)	Gain (dB)
1	8′ FSJ1-50A	Coaxial cable from diplexer to antenna	0.7	-0.7
2	Microwave Circuits D0321581	Diplexer	1.0	-1.0
3	Mini-Circuits ZRL-2400LN+	Low-noise amplifier	1.4	24.8
4	25′ LMR-400	Coaxial cable along roof to diplexer	1.8	-1.8
5	100′ LMR-400	Coaxial cable from indoors to roof	6.0	-6.0
6	Mini-Circuits ZRL-2300+	Pre Amp 1	2.5	21
7	Mini-Circuits ZRL-2300+	Pre Amp 2	2.5	21
8	Mini-Circuits ZFBP-2400-S+	Band-Pass Filter	1.6	-1.6
9	Anaren 10616-10	Directional coupler for power meter	0.7	-0.7
10	RT Logic T400CS	Doppler compensation	11	30
11	Ettus Research USRP B210	Receive radio	6	
		Total	**3.3**	**85.0**

TABLE IV: Receive chain components.

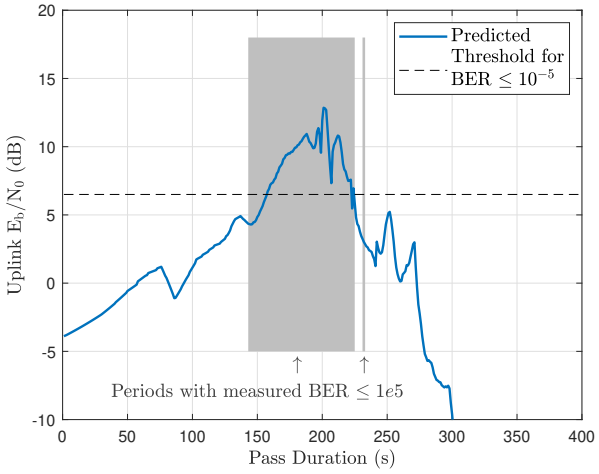

Fig. 8: Predicted uplink E_b/N_0 from STAT with periods where measured BER $\leq 10^{-5}$ shaded in gray.

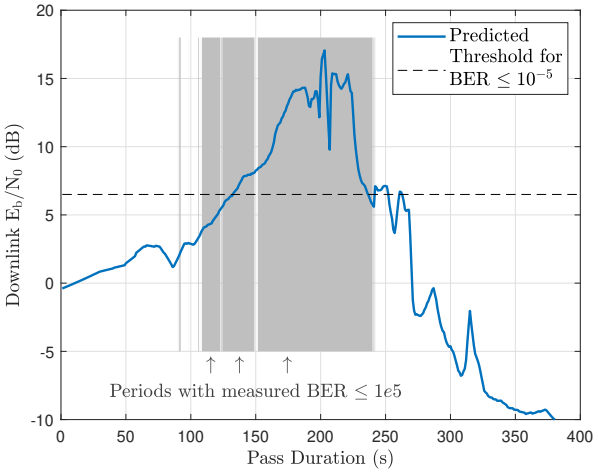

Fig. 9: Predicted downlink E_b/N_0 from STAT with periods where measured BER $\leq 10^{-5}$ shaded in gray.

Predicted E_b/N_0 of the uplink calculated in STAT is shown in Fig. 8. We observe the predicted E_b/N_0 is above the 6.5 dB required to maintain a BER no greater than 10^{-5} during the range of 155 s − 220 s from the start of the pass. The measured BER is less than 10^{-5} over the range of 140 s − 220 s. Fig. 9 shows a similar plot for the downlink. Predicted E_b/N_0 is above the threshold over the range of 120 s − 230 s. With the exception of several small gaps around 120 s and 150 s the measured BER is less than 10^{-5} over this range and slightly outside it. These figures show no significant discrepancy between the predicted and measured BER. We can reasonably conclude that the RF chain is functioning as expected.

VI. Waveform Design

Clearly it would not be acceptable to require that a spacecraft wait for a pass with the unusually high link margin seen in Section V before sending a request for service. With the RF hardware validated, it then became a priority to develop and demonstrate a waveform capable of closing a link with the hemi antenna under the weak signal conditions of a typical pass. This section describes the transmit (downlink) and receive (uplink) waveforms developed for the JPL SDR. The majority of modem functionality is implemented in the radio's field-programmable gate array (FPGA) with some control logic housed on a general purpose processor (GPP). Corresponding waveforms are deployed on the ground, but are sufficiently similar as to not warrant detailed description.

A. Downlink - UIS Request

Data Formatting. Fig. 10 summarizes the transmitter implemented in the JPL SDR. During operation, the Flight Service Manager would generate a UIS request message following the format described in Table I. For the purposes of this test, a known pseudorandom binary sequence (PRBS-11) is transmitted to enable calculation of bit error rate by comparing decoded bits to the known sequence. PRBS bits are packed into a frame following the Advanced Orbiting Systems (AOS) Space Link Data Protocol [26]. The 260-byte AOS frame comprises a 32-bit sync marker, 48-bit header frame, and 2,000 bits of payload (in this case PRBS). Framing is followed by line coding to convert the Non-Return-to-Zero-Level (NRZ-L) bits to Non-Return-to-Zero-Mark (NRZ-M) which removes the need for a phase ambiguity resolution step in the receiver. Finally, a convolutional code ($r = 1/2$) is applied following [27] resulting in a symbol rate of 2 ksym/s.

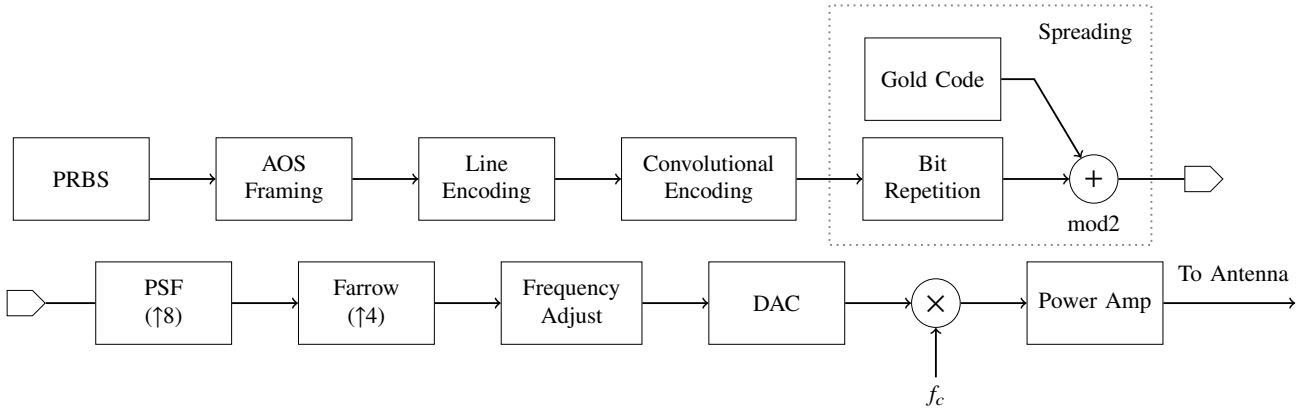

Fig. 10: Simplified transmit chain, implemented on the JPL SDR for the downlink.

Spreading. Transmitting a spread spectrum signal not only provides a multiple access scheme allowing many users to send simultaneous requests, but is required to comply with spectrum regulations. SCaN Testbed is limited in the power flux density (PFD) it can radiate towards earth's surface [28]. The regulation is specified in terms of power per square meter in any 4 kHz reference bandwidth. Fig. 11 shows that at the low symbol rate of 2 ksym/s, the transmitted signal power is concentrated in a very narrow bandwidth (approximately 2.4 kHz) and violates the PFD limit. Multiplying the narrowband signal with a pseudonoise code sequence spreads power over a wider bandwidth and meets the PFD limit. Specifically, the spreading block repeats each information bit and sums the upsampled bit sequence (mod-2) with a Gold code. To speed development, the spreading block is reused from an earlier UIS flight experiment [9].

A spread-spectrum transmission introduces the requirement of a despreading block in the receiver whose performance is proportional to the energy per chip to noise power spectral density ratio E_c/N_0. For fixed transmit power, reducing the chip rate R_c will increase E_c/N_0. For this reason, we operated at the lowest chip rate supported by the existing spreading block R_c = 1.54 Mcps. Analysis shows the chip rate could be as low as R_c = 170 kcps without violating PFD limits. A new block capable of this chip rate would accordingly increase E_c/N_0 by approximately 9.5 dB and therefore improve the performance of the despreader.

Modulation. BPSK modulation is applied by converting the output of the spreading block to binary antipodal chips. By design, the spreading chip rate is exactly $^1/_{32}$ the radio sample rate. Symbols filtered through an 8× interpolating root-raised cosine pulse-shape filter with rolloff (α = 0.35) sufficient to meet the spectral mask for this band [29]. Lagrange interpolation using a Farrow structure upsamples this signal 4× to the radio sample rate f_s.

Doppler Compensation. Before digital-to-analog conversion, the transmit sample stream passes through a frequency adjustment block which serves two functions. First is to digitally compensate for tuning error of the local oscillator

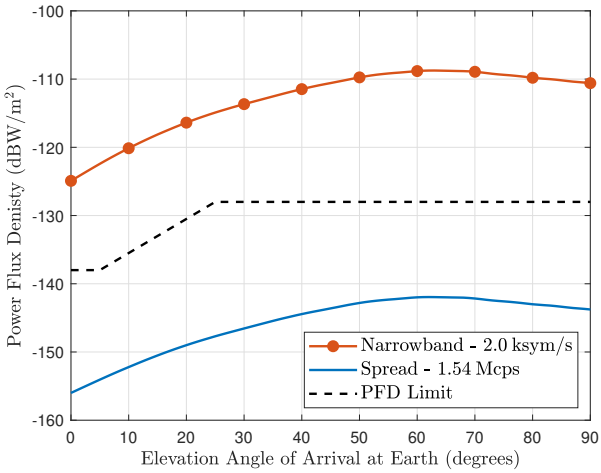

Fig. 11: Approximate power flux density as a function of elevation angle. The narrowband signal (red) exceeds the PFD limit (dashed) but the spread-spectrum signal (blue) does not.

used in upconversion to the passband. Transmit samples are digitally mixed with a numerically-controlled oscillator at a frequency equal to the difference between the desired and actual frequency of the analog local oscillator. Second is to allow for transmit-side Doppler pre-compensation.

A popular technique in SDR receivers is to use received symbols to estimate and correct residual carrier frequency offset. This technique is not practical for this link since the potential Doppler shift range of ±50 kHz is much greater than the symbol rate of 2 ksym/s. Alternatively, pre-compensation can be applied at the transmitter using the frequency compensation block. The Doppler profile can be generated onboard the spacecraft using software described in Section III. The inverse of this profile drives the frequency adjustment block such that the signal received on the ground is at the correct center frequency throughout the pass.

Due to time constraints, transmit-side pre-compensation was not included in the flight experiment described in Section VII. Pre-compensation was instead applied on the ground by loading a Doppler compensation profile into the channel

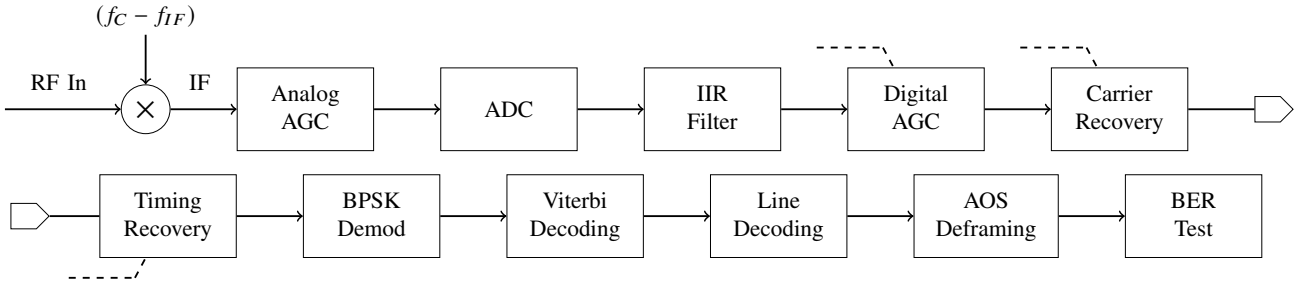

Fig. 12: Simplified receive chain, implemented on the JPL SDR for the uplink. Dashed lines represent configuration connections to/from the GPP.

simulator. In an operational system, this approach would not be practical since the ground station does not know in advance which of several spacecraft in view would send a request. One could envision a system involving multiple software-defined receivers, one for each spacecraft in view, each with a Doppler compensation profile corresponding to that spacecraft. While this approach would require minimal additional processing resources, it is believed pre-compensation on the user spacecraft is the best solution. With the frequency adjustment block and the Flight Service Manager's potential ability to generate Doppler profiles, it should be reasonable and preferable to perform transmit-side pre-compensation.

B. Uplink - UIS Response

Analog Front-End. The uplink signal, which would contain the UIS response in an operational system, originates at the TSIM which also performs transmit-side Doppler pre-compensation. SCaN Testbed receives the uplink signal through the same nadir-facing low-gain antenna with the receive side of a diplexer connected to the signal processing chain shown in Fig. 12. The received signal first passes through the SDR's low noise amplification stage and is downconverted to an intermediate frequency. An automatic gain control (AGC) stage whose level is managed by the FPGA precedes an analog-to-digital converter.

Receiver Filtering. Since the ground equipment will likely send UIS responses to requesting spacecraft one at a time, a code-division multiple access scheme is not required in the uplink. Additionally, no PFD restrictions exist in the uplink direction. For these reasons, a narrowband signal was transmitted. As a result, the JPL SDR does not require a despreading block and the receiver performance is not dependent on E_c/N_0. The digitized signal is first filtered by a 6th-order infinite impulse response (IIR) filter to remove out-of-band energy. The cutoff frequency is equal to the symbol rate plus additional margin to account for residual Doppler shift. Filtered samples are scaled in amplitude by a digital AGC whose operation is discussed later in this section.

Carrier Recovery. The carrier recovery block has two functions: remove residual carrier frequency offset (CFO) and decimate the incoming samples from the radio sample rate f_s to an integer multiple of the symbol rate $f_{sym} = 2\,\text{ksym/s}$. A detailed view of the carrier recovery process is shown in Fig. 13.

The Costas loop takes place at baseband to simplify filtering and leverage existing code. Therefore the incoming samples must be downconverted by mixing with the intermediate frequency, producing in-phase and quadrature components. Operating the Costas loop at the radio sample rate would require large low-pass arm filters. However, if the signal is decimated to the desired sample rate before the Costas loop it would be impossible to correct residual CFO. Therefore decimation is done in two steps: samples are decimated by 32 before the Costas loop and by 48 after the Costas loop. This produces a sample rate of $16 \cdot f_{sym}$ at the output of the carrier recovery block. Specifically, the decimation is done through cascaded integrator–comb (CIC) filters.

A Costas loop phase error detector is used to drive a numerically-controlled oscillator through a loop filter. Each arm contains a low-pass filter and a power estimation block which regularly reports average power in each arm to the GPP. Coefficients describing the loop filter can also be adjusted during operation by the GPP, effectively changing the Costas loop bandwidth dynamically. Initially the loop has a wide bandwidth to aid acquisition. We infer the loop has locked onto the carrier when power in the in-phase arm remains greater than that in the quadrature arm for a certain duration. After acquisition a new set of filter coefficients narrows the loop bandwidth to improve tracking performance.

Timing Recovery. Symbol timing errors are corrected using a Gardner loop. As with the carrier recovery block, loop filter coefficients can be updated from the GPP. A self-normalizing lock detector [30] informs the GPP when timing has been acquired. The GPP then provides a new set of filter coefficients which narrow the loop bandwidth to aid tracking. Finally, the timing recovery block decimates samples to the symbol rate of f_{sym}.

Demodulation. Recovered symbols are fed into a Viterbi decoder. Due to limited development time, the Viterbi block operates on hard bits (recovered by taking the sign of the real component of each received symbol). With additional development, a soft-decision decoder could improve the link margin of a future design by approximately 2.3 dB. Line decoding (NRZ-M to NRZ-L), frame synchronization, and

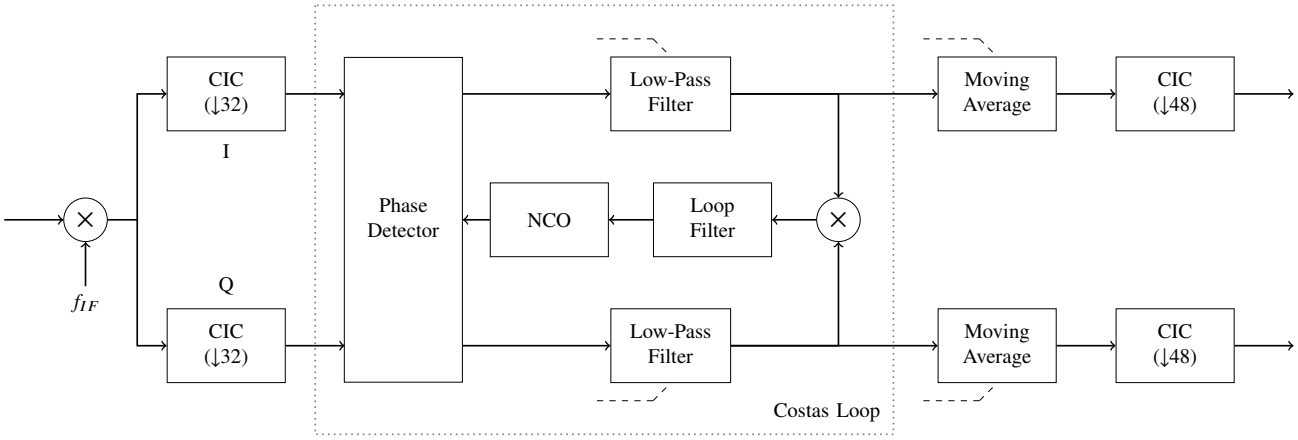

Fig. 13: A detailed view of the carrier recovery block. Dashed lines represent configuration connections to/from the GPP.

AOS deframing produce a stream of PRBS bits at 1 kbps. These bits are compared against an internally-generated sequence and bit error metrics reported to the GPP.

Automatic Gain Control. As shown in Fig. 12, the receiver has both an analog and digital AGC. The AGC drive level is set based on a time-averaged power measurement of the digitized received signal plus noise power. The gain control algorithm seeks to maintain a constant power level, ideally close to but not exceeding the full scale resolution of the ADC. While the analog AGC will maintain the signal plus noise power within a range, the signal power will vary with path loss and fading throughout a pass. Filter coefficients in the receiver are scaled assuming a constant signal power, so a digital AGC to adjust gain based only on signal power is also necessary.

Placed after the IIR filter, the digital AGC multiplies the incoming samples with a scale factor chosen from the set of $\{0.5, 1.0, 2.0\}$. The scale factor is adjusted by the GPP as a function of signal power in the in-phase arm of the Costas loop. When in-phase power exceeds an upper limit the scale factor is reduced. Likewise, in-phase power below a lower limit increases the scale factor. Though the digital AGC implementation is efficient requiring only a bit shift operation, it would be desirable for future versions of the waveform to have finer granularity.

VII. Preliminary Results

The waveform was evaluated during a typical pass over the hemi antenna. While the 18 kbps GGT waveform was suitable for the unusually strong pass described in Section V, it is unable to close the link during any part of this more typical pass - underscoring the need for the waveform design described in the previous section.

A. Uplink

The register value which determines analog AGC gain is shown over the duration of the pass in Fig. 14a. Note that a lower register value produces higher gain. Comparing the register value to the received power at the JPL SDR as predicted by STAT, we observe the AGC approximately tracks the time-varying signal power. Similarly, Fig. 14b compares the digital AGC scale factor to the average in-phase power at the output of the Costas loop. Ground testing experimentally determined that a target range of $\{45, 145\}$ (in unscaled power) results in the best receiver performance. We observe the digital AGC reducing its scale factor when the average power grows greater than 145 and increasing its scale factor when the average power falls below 45.

Testing on the ground with an engineering model of the JPL SDR demonstrated a quasi error free performance down to an input signal level of approximately -130 dBm. This is equivalent to $E_b/N_0 = 9.0$ dB, suggesting an implementation loss of approximately 2.5 dB. Observing the received power prediction in Fig. 14a it should have been possible to maintain mostly error-free data transfer during the first 100 s of the pass. However, the measured on-orbit performance showed several periods of error-free data transmission, each approximately 10 s, with high bit error rates between.

This discrepancy can likely be attributed to the digital AGC implementation. In Fig. 14b we can observe rapid variation in the signal power even when the digital AGC remains at the same scale factor. When the scale factor is adjusted it changes the signal power dramatically: a doubling or halving of the power can be seen after the AGC adjustments at 55 s and 75 s, respectively. This variability likely impacts the ability of downstream blocks to track the signal resulting in the intermittent tracking performance observed. It is likely that the digital AGC adjustments are too coarse and the range over which there is no adjustment is too wide. Future iterations of the design with a more sophisticated digital AGC approach would likely mitigate these problems.

Despite this issue, a total of 2.1 kB of error-free data was transferred during the pass. As discussed in Section III, the UIS responses can be as small as 100 bytes in size. Therefore, even during the brief periods of error-free reception it would have been possible to receive several UIS responses. This result does suggest the concept of sending UIS responses from a hemi antenna to an Earth-orbiting satellite is feasible.

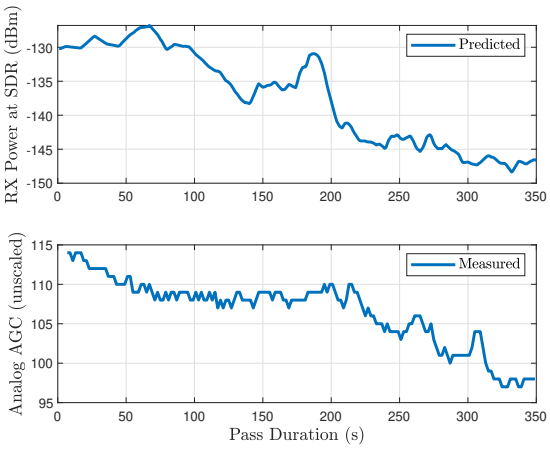

(a)

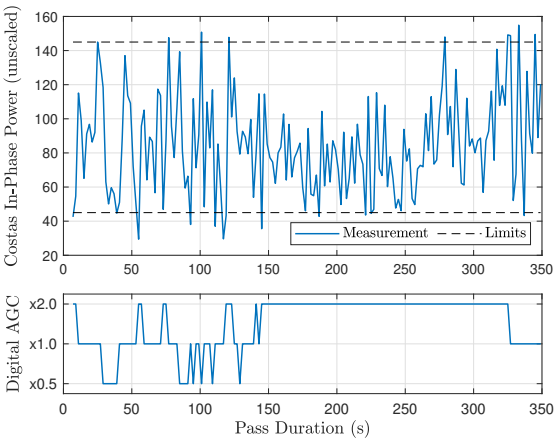

(b)

Fig. 14: AGC performance during the flight experiment. In (a) the analog AGC setting appears to closely track the predicted received signal power at the JPL SDR. In (b) the digital AGC scale factor changes to keep the in-phase power at the output of the Costas loop within a given range.

B. Downlink

With such small packets to transfer (i.e. 65 bytes), it is worth asking if the bit rate could be further reduced to operate with even weaker signals. This was tested in the downlink by setting the bit rate to 0.5 kbps instead of the design target 1.0 kbps. This change resulted in an additional 3 dB of E_b/N_0 as shown in Fig. 15. The link was successfully closed over the first 145 s of the pass, with a total of 9.4 kB of error-free data transferred.

However, tracking was lost after 145 s. Two potential scenarios can explain this result. First, it is possible that the prediction showing a period of increased E_b/N_0 from 150 s – 200 s is not actually correct. This period assumes the structural feature (such as solar arrays) reducing the signal from 100 s – 150 s is no longer present from 150 s until the back lobe of the antenna is reached at 200 s. Due to the complex dynamics of the ISS it is possible this obstruction remained in place, reducing the signal level below what the receiver could decode. We emphasize that STAT provides only estimates and with little link margin a small error in the tool's approximation could lead the user to believe a connection is possible when signal levels are slightly too weak to permit it.

Second, it is observed that the despreader block lost tracking at 145 s which effects the performance of downstream blocks. It is possible that the predicted E_c/N_0 value of −25 dB represents the performance limit of the despreader block. Fig. 15 shows this level is reached at 145 s, around the time when the despreader loses tracking. An alternative despreading technique based on block acquisition of direct-sequence spread spectrum signals could break through this performance limit [31], [32]. Alternatively, the chip rate could be further reduced, down to the limit discussed in Section VI, in order to increase E_c/N_0 and therefore despreader performance. Despite this uncertainty, we emphasize that only a small fraction of the 9.4 kB transferred would be necessary to successfully receive a UIS request. We believe this test validates the concept's feasibility for further development and eventual deployment.

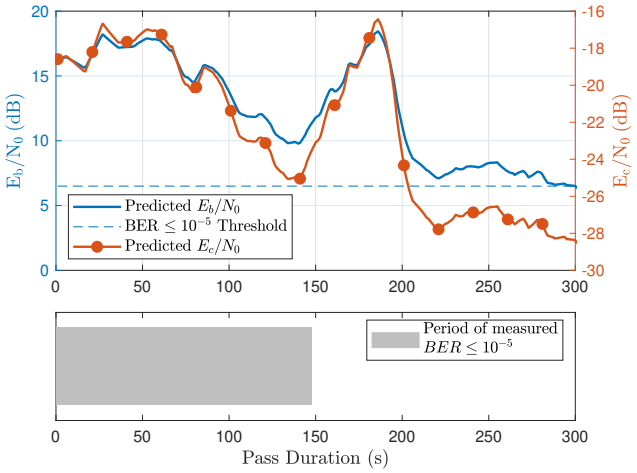

Fig. 15: Predicted downlink E_b/N_0 and E_c/N_0 (top) and the period of time during which the link was closed with a BER $\leq 10^{-5}$ (bottom).

APPENDIX A
COMPARISON WITH DEMAND ACCESS SYSTEM FOR POWER-CONSTRAINED SPACECRAFT

In addition to the flexibility afforded by utilizing a wide network of ground stations for receiving UIS requests, Section I makes the point that small power-constrained satellites may find it easier to send their requests through a ground station rather than closing a link to TDRS. This appendix contains a brief study of this scenario.

While the TDRS multiple access return antenna array is more capable than a hemi antenna on Earth, signals reaching the TDRS satellites in geosynchronous orbit must travel significantly farther. At the S-band frequencies considered in this study, the path loss to TDRS is between 190.5 dB – 192.5 dB

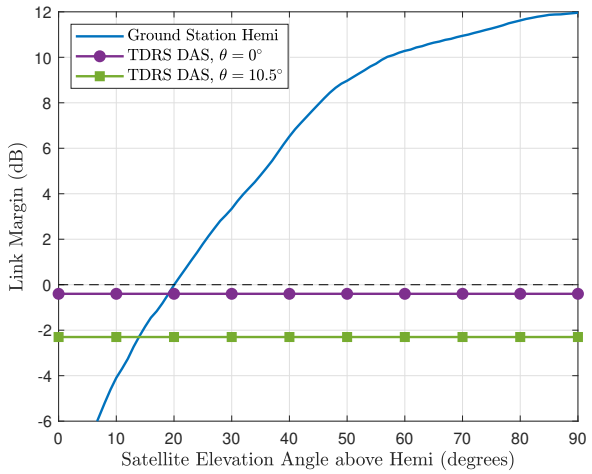

Fig. 16: Link margin versus elevation angle when transmitting to the hemispherical antenna from a spacecraft with 27 dBm EIRP. The overlayed traces show link margin to TDRS when the satellite is directly below TDRS and at the maximum angle (10.5°) of the TDRS field of view.

dependent on the position of the user spacecraft. As demonstrated in [9], SCaN Testbed can close a link to TDRS to send a UIS request. However, less capable spacecraft may not be able to.

Consider a small satellite with a lower power radio and less directional antenna with an EIRP of 27 dBm (this represents a transmitter of 0.5 W and patch antenna of 0 dBi, for example). A link budget analysis shows the spacecraft is incapable of closing an S-band BPSK link to TDRS at 1 kbps with a required E_b/N_0 of 6.5 dB. However, running the link budget analysis with the hemi antenna and RF chain in Section IV shows it is possible to close a link at an elevation angle above 20°. These findings are summarized in Fig. 16.

References

[1] D. J. Israel *et al.*, "Space mobile network concepts for missions beyond low earth orbit," in *International Conference on Space Operations (SpaceOps)*, Marseille, France, May 2018.

[2] M. S. Net, "Support of latency-sensitive space exploration applications in future space communications systems," Ph.D. dissertation, Massachusetts Institute of Technology, 2017.

[3] D. N. Baker *et al.*, "Magnetospheric multiscale instrument suite operations and data system," *Space Science Reviews*, vol. 199, no. 1, pp. 545–575, Mar. 2016.

[4] N. Gehrels *et al.*, "The swift gamma-ray burst mission," *The Astrophysical Journal*, vol. 611, no. 2, pp. 1005–1020, Aug. 2004.

[5] B. P. Abbott *et al.*, "Multi-messenger observations of a binary neutron star merger," *The Astrophysical Journal*, vol. 848, no. 2, p. L12, Oct. 2017.

[6] M. Seablom *et al.*, "Advancing technology for NASA science with small spacecraft," in *32nd Annual AIAA/USU Conference on Small Satellites*, Logan, UT, Aug. 2018.

[7] R. C. Reinhart *et al.*, "Enabling future science and human exploration with NASA's next generation near earth and deep space communications and navigation architecture," in *68th International Astronautical Congress*, Adelaide, Australia, Sep. 2017.

[8] K. M. Coderre *et al.*, "Concept of operations for the gateway," in *International Conference on Space Operations (SpaceOps)*, Marseille, France, May 2018.

[9] D. J. Mortensen, C. Roberts, and R. C. Reinhart, "Automated spacecraft communications service demonstration using NASA's SCaN testbed," in *International Conference on Space Operations (SpaceOps)*, Marseille, France, May 2018.

[10] D. J. Israel, G. W. Heckler, and R. J. Menrad, "Space mobile network: A near earth communications and navigation architecture," in *Proc. IEEE Aerospace Conference*, Big Sky, MT, Mar. 2016.

[11] C. J. Roberts *et al.*, "Preliminary results from a model-driven architecture methodology for development of an event-driven space communications service concept," in *Proc. IEEE International Conference on Wireless for Space and Extreme Environments (WiSEE)*, Montreal, Canada, Oct. 2017, pp. 122–127.

[12] G. Kazz and E. Greenberg, "Mars relay operations: Application of the CCSDS Proximity-1 space data link protocol at mars," in *International Conference on Space Operations (SpaceOps)*, Houston, TX, May 2002.

[13] *Proximity-1 Space Link Protocol*, Consultative Committee for Space Data Systems (CCSDS) Std. 211.0-B-1, Oct. 2002.

[14] R. C. Reinhart and J. P. Lux, "Space-based reconfigurable software defined radio test bed aboard international space station," in *International Conference on Space Operations (SpaceOps)*, Pasadena, CA, May 2014.

[15] *Space Network User's Guide*, NASA Goddard Space Flight Center Std. 450-SNUG Rev. 10, 2012.

[16] T. A. Gatlin and W. Horne, "The NASA space network demand access system (DAS)," in *International Conference on Space Operations (SpaceOps)*, Houston, TX, May 2002.

[17] K. Hogie *et al.*, "TDRSS demand access system augmentation," in *Proc. IEEE Aerospace Conference*, Big Sky, MT, Mar. 2015.

[18] *Near Earth Network User's Guide*, NASA Goddard Space Flight Center Std. 453-NENUG Rev. 2, 2016.

[19] B. Welch, M. Pasecki, and D. Schrage, "Use of a closed-loop tracking algorithm for orientation bias determination of an S-band ground station," in *37th Antenna Measurement Techniques Association Annual Meeting and Symposium*, Long Beach, CA, Oct. 2015.

[20] Federal Communications Commission, "ET Docket 95-18 Second Report and Order," Jul. 2003.

[21] G. Heckler *et al.*, "TDRSS augmentation system for satellites," in *International Conference on Space Operations (SpaceOps)*, Daejeon, Korea, May 2016.

[22] *AS-48915 Series Omnidirectional Conical Spiral Antenna*, Harris Corporation, Oct. 2010.

[23] B. Welch and M. Pasecki, "Earth-facing antenna characterization in complex ground plane/multipath rich environment," in *37th Antenna Measurement Techniques Association Annual Meeting and Symposium*, Long Beach, CA, Oct. 2015.

[24] D. Chelmins, "Glenn Goddard TDRSS waveform 1.1.3 on-orbit performance report," NASA Glenn Research Center, Tech. Rep., May 2014.

[25] NASA Space Telecommunications Radio System, "GRC GSFC TDRSS (GGT) waveform," Source Code Available https://strs.grc.nasa.gov/repository/contents/.

[26] *AOS Space Data Link Protocol*, Consultative Committee for Space Data Systems (CCSDS) Std. 732.0-B-3, Sep. 2015.

[27] *TM Synchronization and Channel Coding*, Consultative Committee for Space Data Systems (CCSDS) Std. 131.0-B-3, Sep. 2017.

[28] *Maximum Permissible Values of Power Flux Density at the Surface of the Earth Produced By Satellites in the Fixed-Satellite Service Using the Same Frequency Bands Above 1 GHz as Line-of-Sight Radio-Relay Systems*, International Telecommunications Union Std. ITU-R SF.358-5, 1995.

[29] *Spectrum Standards: Manual of Regulations and Procedures for Federal Radio Frequency Management (Redbook)*, National Telecommunications and Information Administration (NTIA) Std., Sep. 2017.

[30] Y. Linn, "A self-normalizing symbol synchronization lock detector for QPSK and BPSK," *IEEE Transactions on Wireless Communications*, vol. 5, no. 2, pp. 347–353, Feb. 2006.

[31] L. M. B. Winternitz, W. A. Bamford, and G. W. Heckler, "A GPS receiver for high-altitude satellite navigation," *IEEE Journal of Selected Topics in Signal Processing*, vol. 3, no. 4, pp. 541–556, Aug. 2009.

[32] M. L. Psiaki, "Block acquisition of weak GPS signals in a software receiver," in *Proc. 14th International Technical Meeting of the Satellite Division of The Institute of Navigation (ION GPS)*, Salt Lake City, UT, Sep. 2001.